Four-Dimensional Morphological Evolution of an Aluminum Silicon Alloy Using Propagation-Based Phase Contrast X-ray Tomographic Microscopy

Gulsoy, Emine Begum ; Shahani, Ashwin J ; Gibbs, John W ; Fife, Julie L ; Voorhees, Peter W

DOI: https://doi.org/10.2320/matertrans.M2013225

Materials Transactions, Vol. 55, No. 1 (2014) pp. 161 to 164

Four-Dimensional Morphological Evolution of an Aluminum Silicon Alloy Using Propagation-Based Phase Contrast X-ray Tomographic Microscopy

Emine Begum Gulsoy[1], Ashwin J. Shahani[1,*1], John W. Gibbs[1,*1], Julie L. Fife[2] and Peter W. Voorhees[*2]

[1]*Department of Materials Science and Engineering, Northwestern University, 2220 Campus Drive, Evanston, IL, 60208, USA*
[2]*Swiss Light Source, Paul Scherrer Institut, 5232 Villigen, Switzerland*

Four-dimensional propagation-based phase contrast X-ray tomographic microscopy experiments were performed on an Aluminum-29.9 mass% Silicon alloy during coarsening. Using propagation-based phase contrast, changes in the three-dimensional morphology of primary silicon particles were captured and the resulting evolution of the microstructure is discussed. While morphologies at earlier times are complex, faceted and highly interconnected, the morphologies at later times are less faceted but remain quite complex.
[doi:10.2320/matertrans.M2013225]

(Received June 14, 2013; Accepted October 7, 2013; Published December 6, 2013)

Keywords: *X-ray tomographic microscopy, aluminum–silicon alloy, propagation-based phase contrast, microstructural characterization, coarsening*

1. Introduction

Aluminum–silicon (Al–Si) alloys are very versatile low-cost casting metals and therefore play an important role in industry. The Si-rich alloys are useful due to their excellent hardness and wear properties; however, they present an interesting materials science problem. Al is completely insoluble in Si and this gives rise to the formation of nearly-pure Si particles. These particles are also usually faceted due to either a highly anisotropic solid–liquid interfacial energy or to the interfacial mobility of the Si particles. The as-cast microstructure, consisting of primary Si particles in Al–Si eutectic, is known to be extremely brittle. However, the introduction of very small quantities of additive elements, such as sodium (Na) or strontium (Sr), alters the Al–Si microstructure and therefore improves the mechanical properties, such as ductility.[1–3] While there have been quite a few studies on the effect of various impurities on Al–Si microstructure, the intrinsic growth mechanism of the Si platelets is not very well understood.[4,5]

In most cases, the formation and evolution of the microstructure of Al–Si alloys has been determined using metallography in which the three-dimensional (3D) microstructure must be inferred from a cross section. In addition, since this analysis method is destructive, it is not possible to follow the evolution of individual domains. By contrast, X-ray tomographic microscopy is a nondestructive characterization method that collects data in 3D without damaging the sample (in most cases). Furthermore, in many cases, especially at synchrotron sources, data acquisition can occur at speeds where dynamic information is also accessible and resolved, i.e., 4D imaging. Thus, X-ray tomographic imaging has the capabilities to provide unprecedented information about the evolution of microstructures.[6–8]

Traditionally, absorption-based X-ray tomographic imaging, relies on the density differences between the phases in the sample and has been employed to characterize microstructural evolution. Aluminum–Copper (Al–Cu) alloys are commonly used as pilot systems for such experiments.[6] The large atomic number difference between Al and Cu, when coupled with the concentration difference between the solid and liquid, leads to significant contrast in the tomograms enabling easier processing for robust 3D reconstructions. The atomic numbers of Al and Si, on the other hand, are very similar and therefore are insufficient to provide contrast between phases through traditional absorption-based methods. Thus, propagation-based phase contrast is employed for this study.[9,10] In this approach, the sample remains in the "near-field" regime and the detector is placed at an optimized distance from the sample. This results in images that display edge enhancement, where the phase of the object can be extracted. The challenge with this method is to identify the interfaces, given that they are frequently diffuse, in order to process the data and apply quantitative characterization.

2. Experimental Details

2.1 Alloy preparation

High-purity powders (99.99% Al and 99.9999% Si) were repeatedly melted in a low-pressure argon (Ar) atmosphere to mix and degas the alloys in order to achieve buttons with a composition of 29.9 mass% Si (Materials Preparation Center at Ames Laboratory). The as-cast buttons were machined into cylindrical samples of 1 mm diameter using Electrical Discharge Machining (EDM).

2.2 4D X-ray tomographic microscopy

The experiment was conducted *ex situ* at the TOmographic Microscopy and Coherent rAdiology ExperimenTs (TOMCAT) beamline[11] of the Swiss Light Source (Paul Scherrer Institut, Switzerland) using propagation based phase contrast X-ray tomographic microscopy. The sample coarsened in the solid–liquid state within a custom-made furnace, at 580°C, just above the eutectic temperature. It was then quenched to room temperature and a tomographic scan was taken. The sample was then reheated to 580°C and allowed to coarsen again. This cycle was repeated for eight time steps,

*[1]Graduate Student, Northwestern University
*[2]Corresponding author, E-mail: p-voorhees@northwestern.edu

durations of which are indicated in Table 1. At each time step, 1001 projections were acquired per 180° of rotation. The distance between the sample and the detector was chosen as 110.0 mm, where the data acquisition was optimized to fulfill the near-field condition for phase retrieval in the Al–Si system. A 3D reconstruction of each time step was achieved by first applying the phase retrieval algorithm developed by Paganin *et al.* to the projections,[12] and then baseline reconstructions were obtained using the standard GRIDREC algorithm at TOMCAT.[13,14] It should be noted that the final reconstructions were generated using software developed in-house at Northwestern University. Each reconstructed data set is 1525 × 1525 × 1598 μm, with a voxel size of 0.74 × 0.74 × 0.74 μm.

2.3 Data processing

The primary Si structures in a region of interest (ROI) of 296 × 296 × 159 μm were segmented using a novel hybrid approach. This approach utilizes information from the reconstructions of both absorption-based and phase retrieved images at a single object-detector distance, in a manner similar to the so-called fusion algorithm.[15,16] For reconstructions each 2D section of the 3D data set was segmented individually rather than directly in 3D. These binarized 2D sections were then combined to reveal the 3D microstructure. Three time steps were reconstructed in 3D and the cross-sections from these time steps are shown in Figs. 1(a)–1(c). Results are shown in Fig. 2, using two view angles 180° apart.

Table 1 The coarsening protocol for each sample. Each time listed, corresponding to the images shown in Fig. 1 respectively, represents how long the sample was held isothermally at 580° prior to collection of tomograms. If the times are added together, this table indicates the total time the sample was coarsened (110 min).

Time step	t_0	t_1	t_2	t_3	t_4	t_5	t_6	t_7
Time in furnace, t/min	As-cast	10	10	10	10	10	30	30

3. Results and Discussion

The effect of coarsening on the morphology of the microstructure is shown in Fig. 1. These cross-sections provide a qualitative observation of the change in alloy microstructure after a series of coarsening times.

Two main types of morphologies can be observed in Fig. 1: the dark gray regions in the images are the primary Si particles. The light gray matrix consists of fine acicular-shaped Si and Al that make up the eutectic phase. This eutectic phase is visible due to the *ex situ* nature of the experiments; as discussed in section 2.2, the samples were removed from the furnace and quenched to room temperature before the tomograms were collected at each time step. Thus, the liquid that was present at the coarsening temperature results in the eutectic phase in the reconstructions. The black regions, especially the large ones observed at later times, are voids resulting from casting defects.

Previous *in situ* TEM studies conducted by Moorthy and Howe showed that while primary Si laths grow highly faceted, the dissolution results in smoother, less faceted surfaces.[17] It is also well known that the {111} planes of Si have extremely low mobility, due to the difficulty of creating new atomic steps on the surface. However, if there are defects that intersect the interface, such as a twin, they can provide a source of steps that allow the structure to evolve. Since the evolution of the structure is driven by interfacial energy, the driving forces are small and thus the kinetic limitations of step formation can be particularly difficult to overcome without the benefit of defects.

The as-cast microstructure, shown in 2D in Fig. 1(a) and in 3D in Figs. 2(a), 2(d), shows a high number of facets and sharp corners. As the system coarsens, the sharp corners and edges in the structure tend to disappear. Structures grow less interconnected and less complex but some degree of faceting is still observed at later times. This suggests the presence of low energy, low mobility {111}-type facets on the solid that do not evolve as quickly as the other orientations.

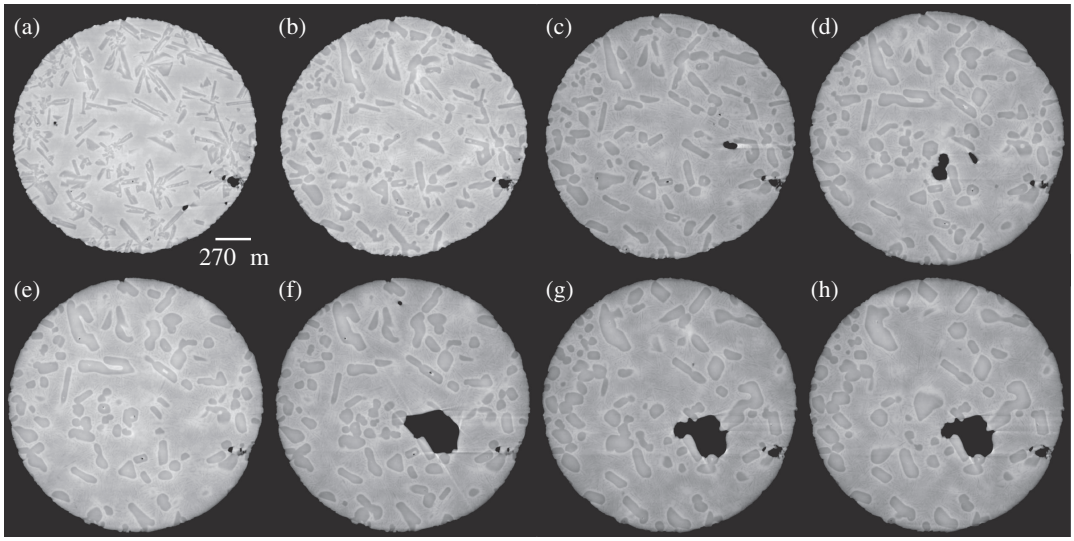

Fig. 1 Phase images of Al–29.9 mass% Si structure coarsening in time. (a) As-cast microstructure is shown. Samples were coarsened in the furnace for (b)–(f) 10 min, (g), (h) 30 min for a total coarsening time of (b)–(h) 10, 20, 30, 40, 50, 80, 110 min respectively.

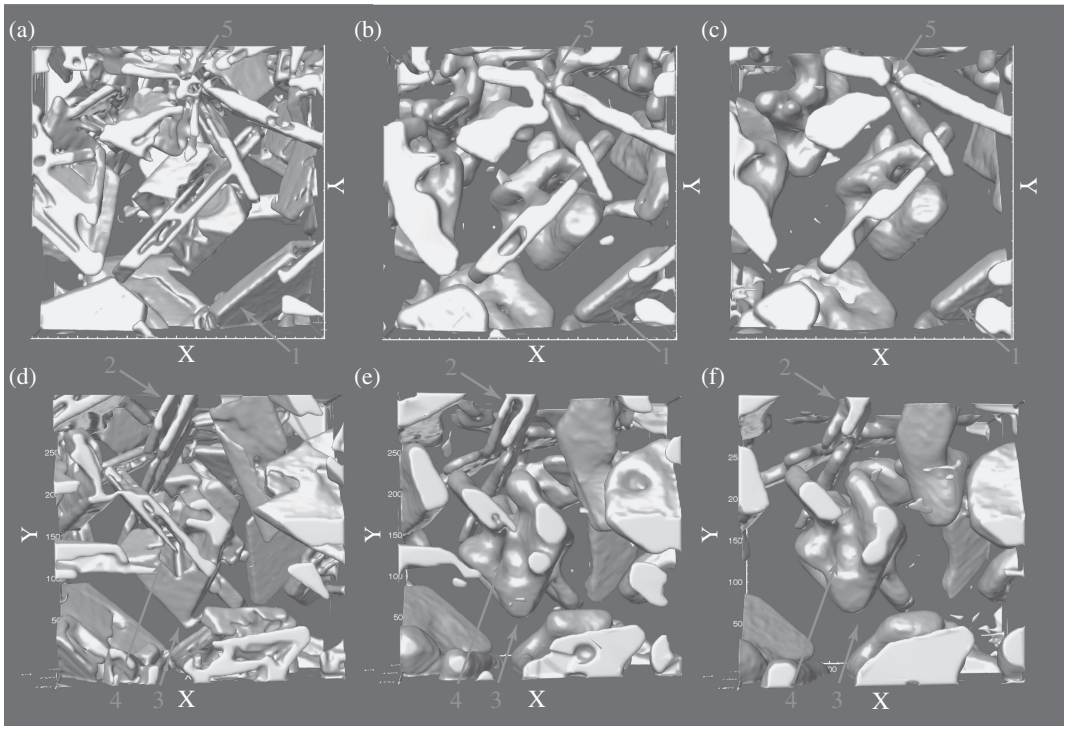

Fig. 2 3D reconstructions of a ROI from the microstructure, showing a view of (a)–(c) the back and (d)–(f) the front of the ROI respectively at each time step. Shown is the microstructure, (a), (d) as-cast, (b), (e) after 10 min of coarsening and (c), (f) after 20 min of coarsening. Images correspond to a region of 296 × 296 × 159 μm.

In Fig. 2, arrow 1 follows a Si lath during time steps, t_0, t_1 and t_2. It is apparent that while the thickness of the lath remains constant, the length of the lath decreases. It is also observed there is strong faceting at time step t_0, indicated by sharp edges that become rounded in times t_1 and t_2. Interfacial kinetics depend on the orientation of the interface, or on the interfacial energy. If the shape of the laths were indeed a Wulff shape, the shape that minimizes the interfacial energy of the lath, then the ratio of the width to the length of the lath would remain constant in time and only the volume of the lath would change. As this is not the case, it is clear that the structure is not evolving through a series of equilibrium shapes. This is consistent with previously reported observations in the literature of {111} facets being favored during Si growth.[5] The broad face of the lath, which is suggested to be of {111} type, appear to be growing much slower with respect to the edges of the lath, giving rise to the observed structural changes.

In Fig. 2, arrow 2 follows a similar lath formation but with a different local environment where two parallel laths are adjacent to one another. The same phenomenon is observed, where the length of the lath evolves faster than the thickness of the lath. Related structures have been previously reported in the literature to be associated with twin boundaries.[5] The twin boundary between the two laths acts as a source of steps and results in an energetically favorable environment for the two laths to merge while keeping their broad facets with the liquid. However, in this classical reentrant twin Si growth process, the reentrant interfaces are {111}, which would lead to a V-shaped interface with the twin at the root of the V. At time step t_2, a single lath has almost formed at the expense of the two laths in the previous time steps.

Another example of the change in faceting with time is shown by arrow 3 in Fig. 2. The sharp edges of the primary Si structure, clearly observed at time step t_0, are increasingly rounded at time steps t_1 and t_2. This is consistent with Moorthy and Howe's observation that interfaces become less faceted during melting.[17] It is also worth pointing out that this particular Si structure is much more complex than a simple lath structure such that it is made of several single laths connected in a non-regular fashion. It can observed in Figs. 2(d)–2(f) that an elongated hole is formed in the middle of the particle denoted by arrow 4. Such structures are generally considered energetically unfavorable. A pair of sharply intersecting plates, as seen at the initial time step t_0, give rise to the elongated hole formation at time steps t_1 and t_2. The growth along the intersection plane of the platelets is faster than that of the plate surfaces, resulting in rounding around the intersection, therefore an elongated hole is forced to form as an intermediate structure during coarsening.

Figure 2, arrow 5, shows the tip of a typical star-shaped morphology that has been commonly observed in Al–Si alloys and has been found to be preferred over random plate formation.[5] This particle is located at the edge of the reconstructed ROI, as can be seen through the flat surfaces it makes with the viewing edge of the reconstructed space. As a result, the reconstruction cannot determine the global morphology of the object. At least six side-plates are present at t_0. At t_1 and t_2, the number of side plates decreases to five and four respectively. This type of star-shaped morphology, which has been shown to accommodate up to eight side-plates, has been previously linked to twinning about {210} planes for alloy compositions with lower Si content.[4] Further investigation and a larger ROI reconstruction is needed to determine the angles between laths.

4. Conclusions

The *ex situ* evolution of the coarsening microstructure of Al–29.9 mass%Si was captured using 4D propagation-based phase contrast X-ray tomographic microscopy. Complex, highly-interconnected primary Si morphologies were observed in the as-cast microstructure. While the complexity of the structures decreased with longer coarsening times, some faceting was still apparent at later times. The qualitative observations are in line with previous observations in literature using different experimental techniques. We find that domains tend to round during coarsening, and that there are interfaces with very low mobility present in the structure. Further studies of the coarsening mechanisms on 3D morphology is expected to reveal a greater understanding of the system.

Acknowledgements

This work was supported by DOE Stewardship Science Graduate Fellowship (JWG). The data was collected under the support of the U.S. Department of Energy, Office of Basic Energy Sciences, Division of Materials Sciences and Engineering under award DE-FG02-99ER45782 and reconstructed under the support of the AFOSR under award FA9550-12-1-0458. This work was supported by the 176th Committee on Process Created Materials Function of the Japan Society for the Promotion of Science (JSPS).

REFERENCES

1) H. Liao, Y. Sun and G. Sun: Mater. Sci. Eng. A **335** (2002) 62–66.
2) S. C. Flood and J. D. Hunt: Metal Science **15** (1981) 287–294.
3) K. Nogita, J. Drennan and A. K. Dahle: Mater. Trans. **44** (2003) 625–628.
4) M. G. Day and A. Hellawell: Proc. R. Soc. A **305** (1968) 473–491.
5) R. E. Napolitano, H. Meco and C. Jung: JOM **56** (2004) 16–21.
6) D. J. Rowenhorst and P. W. Voorhees: Ann. Rev. Mater. Res. **42** (2012) 105–124.
7) J. L. Fife and P. W. Voorhees: Acta Mater. **57** (2009) 2418–2428.
8) O. Ludwig, M. Dimichiel, L. Salvo, M. Suery and P. Falus: Metall. Mater. Trans. A **36** (2005) 1515–1523.
9) P. Cloetens, R. Barrett, J. Baruchel, J. P. Guigay and M. Schlenker: J. Phys. D **29**.
10) A. Snigirev, I. Snigireva, V. Kohn, S. Kuznetsov and I. Schelokov: Rev. Sci. Instrum. **66** (1995) 5486–5492.
11) M. Stampanoni, A. Groso, A. Isenegger, G. Mikuljan, Q. Chen, A. Bertrand, S. Henein, R. Betemps, U. Frommherz, P. Bhler, D. Meister, M. Lange and R. Abela: Proc. SPIE **6318** (2006) 63180M.
12) D. Paganin, S. C. Mayo, T. E. Gureyev, P. R. Miller and S. W. Wilkins: J. Microscopy **206** (2002) 33–40.
13) B. A. Dowd, G. H. Campbell, R. B. Marr, V. V. Nagarkar, S. V. Tipnis, L. Axe and D. P. Siddons: SPIE's International Symposium on Optical Science, Engineering, and Instrumentation, (International Society for Optics and Photonics, 1999) pp. 224–236.
14) F. Marone and M. Stampanoni: J. Synchrotron Rad. **19** (2012) 1029–1037.
15) A. J. Shahani, E. B. Gulsoy, J. Gibbs and P. W. Voorhees: Manuscript in Preparation.
16) G. Lovric, S. F. Barre, J. C. Schittny, M. Roth-Kleiner, M. Stampanoni and M. R. Mokso: J. Appl. Crystallogr. **46** (2013) 856–860.
17) S. K. Eswara Moorthy and J. M. Howe: Metall. Mater. Trans. A **42** (2011) 1667–1674.